The yielding of defect-entangled dispersions in a nematic solvent

The yielding of defect-entangled dispersions in a nematic solvent.

N.Katyan,[1] A. B. Schofield,[1] and T.A.Wood[1]

School of Physics and Astronomy, University of Edinburgh, EH9 3FD, Edinburgh, U.K.

(Dated: 9 August 2021)

Oscillatory rheology, at both small (SAOS) and large (LAOS) amplitude, was performed to measure the dynamic response of a soft-solid, formed on dispersing colloids into a thermotropic nematic liquid crystal at volume fractions $\phi > 18\%$. Due to weak homeotropic anchoring of nematogens at colloid surfaces, a Saturn-ring defect-line, known as a 'disclination', encircles each particle and entangles with neighbouring Saturn-ring disclinations[1]. We present the first experimental investigation of the yielding behaviour of the resulting gel to reveal the underpinning physics. Results reveal the frequency response of the composite is independent of the volume fraction ϕ; an indication that the dispersed phase simply increases the density of disclinations spanning the composite without further effect. Beyond the linear viscoelastic regime (LVR), LAOS experiments indicate the composite is an elastoplastic fluid exhibiting both strain-hardening and shear-thinning behaviour, with Chebyshev coefficients $e_3 > 0$ and $v_3 < 0$ respectively. We deduce that the disclination density n is constant until the strain amplitude is sufficient to break disclinations leading to shear-thinning behaviour beyond the LVR. A simple theory is introduced revealing that the Ericksen number E_r determines the onset of flow, when $E_r > 1$, generating a strain-hardening response since the Frank elasticity resists reorientation of molecular alignment within confined nematic domains. Above a critical frequency ω_c the loss modulus G'' increases slowly due to enhanced viscosity within confined nematic domains, $G'' \propto \omega^{1/2}$ [2]. Observation of this behaviour in a small-molecule nematic solvent provides insights into the physics of flow behaviour in other, more complex, defect-mediated liquid crystalline structures exhibiting similar properties [3–5].

I. INTRODUCTION

Physical stability, preventing sedimentation or creaming, is key to the shelf-life of formulations and composites. Stability can be assured if the storage modulus G' describing the elasticity, is higher than the loss modulus G'' describing the viscous properties, of a fluid to timescales longer than a year, equivalent to applied frequencies $\omega < 10^{-7}$ rad/s. Non-equilibrium structures such as gels and glasses are characterised by a yield stress that allows dispersed colloids to remain distributed homogeneously over a long timescale, ideally years. The microstructure can rearrange if the interaction energy between neighbouring particles is close to the thermal energy, $U \sim k_B T$. This is common for colloid-polymer mixtures, typically used in agrochemical and ink formulations, and renders them sensitive to phase separation [6]. Over twenty years ago, Poulin *et al.*, dispersed colloids within a thermotropic nematic liquid crystal and found that the interaction energy $U > 100 k_B T$ overcomes Brownian motion [7] leading to the formation of colloid chains and aggregates. A decade ago, a novel defect-stabilised gel was discovered with $G' > 10^3$Pa, when colloids are mixed directly into a nematic phase at volume fractions $\phi > 18\%$ [1]. For the first time we explore, systematically, the yielding behavior of these composites using small-amplitude (SAOS), and large-amplitude (LAOS), oscillatory strain measurements using a strain-controlled rheometer and we present a simple theoretical model to explain the behaviour.

Frequency sweep measurements provide vital insights into the underlying physics determining gel formation, for example, the cross-link density in polymeric gels [8] and rubbers [9] and the strength of the interaction between the interface and matrix in dispersions [10]. For strain-controlled deformation, the imposed strain takes the form $\gamma(t) = \gamma_0 \sin\omega t$ which, consequently, imposes the strain rate $\dot{\gamma} = \gamma_0 \omega \cos\omega t$ and the resulting oscillatory shear stress $\sigma = G^* \gamma$ can be recorded by a rheometer. The complex shear modulus $G^* = G' + iG''$ with the storage G' and loss G'' moduli as its real and imaginary parts. In the linear viscoelastic regime (LVR), G' and G'' describe the strength of the elastic (solid-like) and viscous (liquid-like) responses of the sample, respectively [11]. When a dispersed phase provides mechanical reinforcement to the surrounding matrix, it is considered an 'active filler' resulting in an increase in G' with volume fraction ϕ [12]. The converse occurs in the case of an inactive or 'passive' filler which has little affinity for the environment it is in. Within a nematic phase, rheology measurements have shown $G' \sim \phi^{2.5}$ which suggests that colloids may act as 'active' fillers[1]. For polymeric systems, it is known that the number density of gel-strengthening agents (e.g. the cross-link density [8]) increases the critical

frequency ω_c at which the gel yields, where $G' = G''$. Motivated to explore whether the volume fraction of colloids shifts ω_c we measured the frequency dependence across the range $20\% \leq \phi\% \leq 45\%$ of colloids dispersed in a nematic liquid crystal.

More in-depth insights into yielding behaviour can be revealed through large amplitude oscillatory strain (LAOS) measurements, having been applied to a wide variety of soft matter systems including polymer solutions [13], drilling fluids [14], dense suspensions [15] and worm-like micelles [16]. When the oscillatory strain amplitude is large enough to disrupt the structure of the samples, the resulting stress is no longer purely sinusoidal but includes higher harmonic frequencies. We present the first LAOS measurements and analysis on colloidal dispersions in nematic liquid crystals.

Before considering the physics of the composite, we must first consider the flow behaviour of a pure nematic liquid crystal, itself a complex fluid. A thermotropic nematic liquid crystal is composed of rod-like molecules, nematogens, preferring to orient along a direction known as the 'director', **n(r)** [17]. A pure nematic phase has no intrinsic positional order, only orientational order, and appears liquid-like with $G'' \gg G'$ at all frequencies. At a surface, nematogens are held with an anchoring energy W and are unable to align with the bulk director [17]. The resistance of the local director to deformation is dependent on the type of distortion, e.g. splay, twist and bend, and is described by the Frank elastic constants, k_1, k_2 and k_3, respectively. The orientation of the director with respect to the direction of flow affects the measured viscous response (described by the Miesowicz viscosities, η_1, η_2 and η_3) [18] and generates an elastic response such that the storage modulus G' is slightly elevated (although $G' < G''$) close to the resonance frequency $\omega_r \sim 18.65\frac{k_1}{\eta_1 h^2}$, where h is the smallest dimension of the geometry [19–21]. The resonance frequency $\omega_r \sim 0.005$rad/s is towards the lower limit available for practical rheology experiments, calculated using typical values for a thermotropic nematic material (5CB), having $k_1 = 5.5$pN and $\eta_1 = 88$mPa.s, measured between a typical rheometer geometry gap of $h = 0.5$mm. The full behaviour is explained by the universal theoretical description provided by Rey *et al.* which is valid for a broad range of nematic materials including those that are flow-aligning and tumbling, polymeric and lyotropic [21] and confirms that the viscous properties dominate, such that $G'' > G'$, while $G'' \sim \omega$ for all frequencies. The director of a nematic liquid crystal rotates in phase with the shear rate for low frequencies ($\omega < \omega_r$) generating $\tan\delta = G''/G' \sim \omega^{-1}$, classic behaviour for a viscous fluid in the terminal regime. At frequencies above the resonance frequency ($\omega > \omega_r$) the director rotates in phase with the shear strain so that $\tan\delta \sim \omega^{1/2}$ [22, 23]. Although the flow

behaviour in the presence of colloids has not been modelled to date, Burghardt warned in 1990 that "in the presence of monodomains, the estimated time scale for director relaxation becomes short enough that distortional elastic effects may contribute significantly to the macroscopically observed viscoelastic response" [19].

When a spherical colloid is dispersed in a nematic liquid crystal, nematogens can lie parallel or perpendicular (homeotropic) to the colloid surface [7, 17, 24]. In general terms, the type of defect induced by colloids in nematic liquid crystal depends upon the strength of the generalized elasticity K, of the nematic phase, the particle radius r, and strength of anchoring W, of mesogens at the surface of the colloids [7, 17]. Weak homeotropic anchoring with $\frac{Wr}{K} \ll 1$ induces a quadrupolar director field, represented in two dimensions in Fig.1a, which generates a 'Saturn-ring' defect-line, or 'disclination' that encircles the colloid, as shown in Fig.1b, at an orientation normal to the local director orientation. This type of disclination has a topological charge of $s = -\frac{1}{2}$ and, typically, a core radius $r_c \sim 5$nm for a thermotropic nematic liquid crystal [25]. Within the quadrupolar director field, colloids experience highly anisotropic interactions, $|U| \sim 10^3 k_B$T [26], with both attractive and repulsive components depending on the relative orientation of neighboring colloids and the far-field director [7, 27–29]. Anisotropic interactions result in the formation of clusters [26] and the deep potential suppresses Brownian motion. In close proximity, 'Saturn-ring' disclinations can entangle with a range of possible topological configurations of which the most common, the 'figure of eight' disclination (shown in Fig.1c), provides a centre to centre particle separation of $d_0 = 1.1D$ where D is the particle diameter [30]. Each disclination carries a line tension T[25] where

$$T = \pi K s^2 ln \frac{L}{r_c} + \pi \sigma_c r_c^2. \tag{1}$$

The energy density, σ_c of the disclination is often approximated as $\sigma_c \approx K/r_c^2$ where r_c is core radius [25]. The linear dimension, L, desribes the region of director deformation around the disclination and typically $L \sim 10\mu$m while $r_c = 5$nm. For a typical thermotropic liquid crystal $T \sim 100$pN for an $s = -\frac{1}{2}$ disclination [25]. Above a critical volume fraction ϕ_c, Saturn-ring disclinations connect and percolate throughout a composite thus providing rigidity, as revealed through computer simulation ($\phi_c = 15\%$) and measured through rheology measurements ($\phi_c = 18\%$) [1]. The storage modulus $G' \sim nT/A$ where n is the number of disclinations spanning a slab of the composite of area A. Equivalently, $G' \sim T/d_{net}^2$ where d_{net} is the average distance between disclinations spanning the composite [31]. Spaces within the colloidal network are filled with pure nematic solvent of a typical lengthscale a, as illustrated in Fig.1e and by Kumar *et al.* [32]. We present

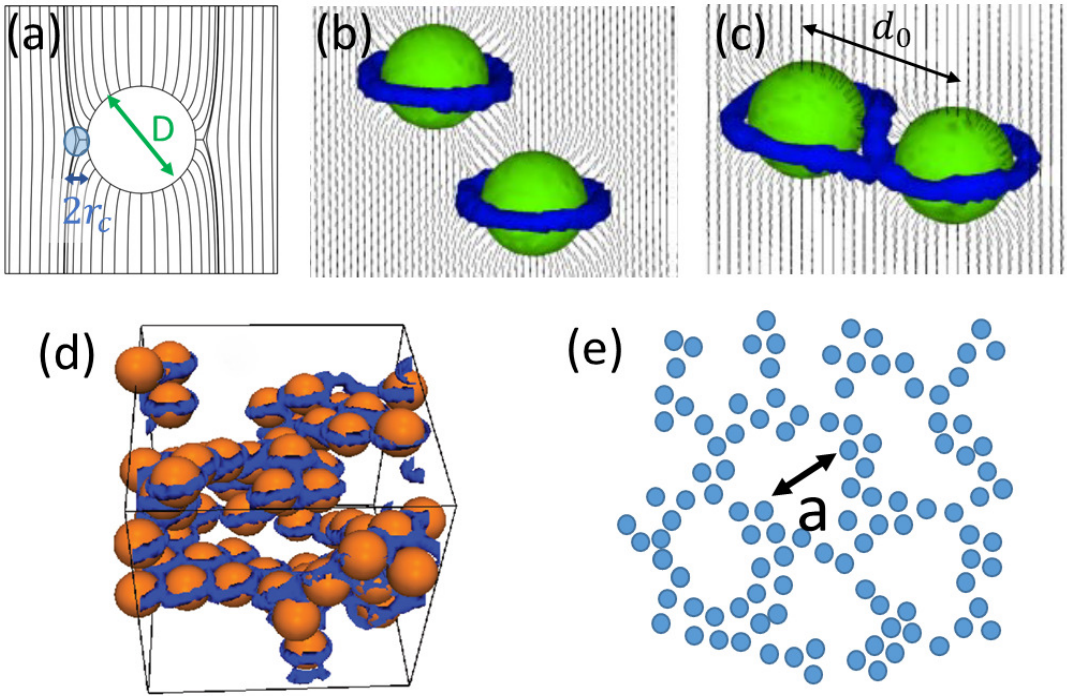

FIG. 1. a) The director field, as seen in two dimensions, around a particle generating weak homeotropic anchoring (reprinted from [33]), labelled to indicate the colloid diameter D and disclination radius r_c. b) In three dimensions, a 'Saturn-ring' disclination encircles the waist of each colloid (reprinted from [30]) and c) neighbouring Saturn-ring disclinations can entangle to form a quasi-stable configuration, here shown in the 'figure of eight' configuration (reprinted from [30]), with colloid centres separated by a distance d_0. d) For high volume fractions $\phi > 18\%$ disclinations wrap around particles forming a network to generate continuous disclination routes across the sample (reprinted from [1]) to leave e) pure nematic regions of lengthscale a within the network.

experimental data from microscopy and SAOS and LAOS rheology measurements to probe the structure and dynamic response of dispersions in a nematic solvent at $\phi > 20\%$. A new theoretical description combines existing physical principles, including the total line tension from disclinations and the enhanced viscosity of nematic phases in confinement, to describe the flow behaviour of this unusual class of composite.

II. MATERIALS AND METHODS

A. Materials

Poly(methyl methacrylate) particles (PMMA) sterically stabilized by chemically grafted poly(12-hydroxy-stearic acid) (PHSA) molecules were prepared and dispersed in dodecane [34]. Particles were labeled using a fluorescent monomer (7-nitrobenzo-2-oxa-1,3-diazol-methyl-methacrylate) which was chemically attached to the PMMA [35]. The particle diameter, $D = 1.17 \pm 0.12 \mu$m, was determined on dilution using dynamic light scattering. The solvent was replaced through ten cycles of centrifuging, discarding the solvent and re-dispersing in hexane. Finally, the sediment was dried thoroughly at 50°C for >3 days under vacuum to create a dry powder of particles of density $\rho_p = 1.18$ g/cm^3, literature value.

The thermotropic nematic liquid crystal, 4-cyano-4'pentylbiphenyl (5CB), was purchased from Kingston Chemicals (UK) and used as received. It is reported to change from a crystalline to nematic state at 22.8°C and to an isotropic state at 35.4°C [36]. At 25°C, the splay, twist and bend elastic constants are 5.5 pN, 4.5 pN and 9.9 pN, respectively [37]. The Miesowicz viscosities for 5CB are reported as $\eta_1 = 88$ mPa.s, $\eta_2 = 94$ mPa.s and $\eta_3 = 15$ mPa.s at 31°C [38] and the rotational viscosity $\gamma_r = 81$ mPa.s at 24°C [39].

To prepare dispersions, the dry PMMA-PHSA powder was added to 5CB (density $\rho_{lc} \sim 1$ g/cm^3) at the appropriate weight fraction and sonicated for 30 minutes at ~ 37°C before being stirred vigorously by hand using a spatula at room temperature for 5 minutes before use. A range of volume fractions, $20\% \leq \phi \leq 45\%$ were prepared. It is known that micron-scale PMMA-PHSA colloids generate weak homeotropic anchoring of nematogens at the surface leading to a quadrupolar director field, necessary for Saturn-ring disclinations to form [1].

Experiments were not performed above $\phi = 45\%$ since samples with a higher volume fraction had a crumbly texture and were difficult to handle. The entangled 'figure of eight' structure surrounding two colloids has been predicted to hold colloids at an interparticle separation of $d_0 = 1.1D$ [30]. Presuming that particles could be arranged into a random close packing structure with $\phi_{max} = 64\%$, we might expect that the limiting volume fraction to be $\phi_{limit} \sim 0.64/1.1^3 = 48\%$. The theoretical limit of $\phi_{limit} = 48\%$ is very close to the limit discovered for practical experiment.

B. Methods

Microscopy: In order to image the director field surround a single colloid dispersed in 5CB, two glass cover-slides were spin-coated with 1%wt poly(vinyl alcohol) solution dissolved in ethanol, allowed to dry overnight at 45°C and rubbed with velvet in one direction, to achieve uniform and planar alignment of the director on the glass. Spacers were created using 10μm diameter glass spheres dispersed in ultra-violet curing glue, to secure two opposing glass slides. A dilute dispersion ($\phi = 0.1\%$) of PMMA-PHSA particles in 5CB was drawn into the home-made cell through capillary action. To perform microscopy on concentrated dispersions ($\phi > 20\%$), a sample was loaded onto an untreated glass slide and enclosed by a second untreated cover-slide. An inverted microscope (Axio Observer, Carl Zeiss Microimaging, Inc.), equipped with an oil-immersion $\times 63$ magnification objective lens was used to image the sample. In confocal mode, a Zeiss LSM 700 laser scanning microscope was used with the 488 nm laser line selected to excite the fluorescent signal from the particles, collected in reflection. In polarized optical microscopy (POM) mode, a polariser orthogonal to the laser light polarisation was used to image the transmission of light through a birefringent sample.

Rheology: Dispersions were stirred by hand prior to measurement in the rheometer. For ease of use, the majority of rheology measurements were performed between sand-blasted steel surfaces of a 40 mm parallel-plate geometry at a gap of h=500$\pm$1 μm on a strain-controlled rheometer, ARES G-2 (TA Instruments). Molecular dynamics simulations indicate that 5CB prefers random planar alignment on atomically-smooth iron surfaces [40]. Random alignment will generate discontinuities between regions of uniform alignment, some of which will nucleate $s = -\frac{1}{2}$ disclinations. Confocal imaging (not shown) reveals a sandblasted steel surface has asperities of the order of 10μm which is sufficient for the gel to fill the valleys to prevent surface-slip and allow $s = -\frac{1}{2}$ disclinations generated by particles to connect with those generated by the sand-blasted steel surface. The geometry was preheated and maintained at 25°C for all measurements. A pre-shear of $0.1/$s was applied for up to 30 seconds before a measurement protocol proceeded. For comparison, some measurements were performed using a 60mm 2° colloid-coated cone-plate geometry, with a truncation gap of 52μm, on a stress-controlled rheometer, AR2000 (TA Instruments). In this case, the smooth steel surfaces of the geometry were pre-treated by spin-coating a $\phi = 30\%$ PMMA-PHSA dispersion in hexane onto the geometry surfaces, sintering, and then cooling to create a rough surface promoting homeotropic alignment from each colloid sintered onto the geometry.

The following rheological protocols were applied:

Small amplitude oscillatory shear (SAOS): Strain sweep tests were performed for all volume fractions $20\% < \phi < 45\%$ for strain amplitudes ranging from $0.01\% < \gamma_0 < 10\%$ at a fixed frequency of $\omega = 2\pi$rad/s. Measurements were performed on the ARES G-2 strain-controlled and the AR2000 stress-controlled rheometer. At least 6 cycles were measured for each data point. Frequency sweep tests were performed in the frequency range of $2 \times 10^{-3} < \omega < 300$rad/s on the ARES G-2 rheometer for each volume fraction and for $0.1\% < \gamma_0 < 4\%$. A single $\phi = 30\%$ sample was tested to very low frequencies within the range of 4×10^{-4} to 4×10^{-3} rad/s.

Large amplitude oscillatory shear (LAOS): Only the strain-controlled ARES G-2 rheometer was used for LAOS measurements. Using the correlation data acquisition mode in the TRIOSv5 software (TA Instruments) the raw strain and stress was collected during 6 full cycles at 2π rad/s. The stress response can be represented by Fourier series in elastic and viscous forms [13]:

$$\sigma(t,\omega,\gamma_0) = \gamma_0 \sum_{n=odd} [G'_n(\omega,\gamma_0)sin(n\omega t) + G''_n(\omega,\gamma_0)cos(n\omega t)] \tag{2}$$

$$\sigma(t,\omega,\gamma_0) = \dot{\gamma}_0 \sum_{n=odd} [\eta'_n(\omega,\gamma_0)sin(n\omega t) + \eta''_n(\omega,\gamma_0)cos(n\omega t)]. \tag{3}$$

Cho *et al.* generalised linear viscoelastic theory for LAOS proposing that the general stress could be decomposed into an elastic stress response, $\sigma'(t)$ and a viscous stress response $\sigma''(t)$ such that $\sigma(t) = \sigma'(t) + \sigma''(t)$ [41]. Using these definitions, Ewoldt *et al.* proposed a new framework with Eqs.2 and 3 rewritten as:

$$\sigma' = \gamma_0 \sum_{n=odd} G'_n(\omega,\gamma_0)sin(n\omega t) \tag{4}$$

$$\sigma'' = \dot{\gamma}_0 \sum_{n=odd} G''_n(\omega,\gamma_0)cos(n\omega t) \tag{5}$$

where the nth order Chebyshev polynomials of the first kind, $Tn\left(\frac{\gamma}{\gamma_0}\right)$ and $Tn\left(\frac{\dot{\gamma}}{\dot{\gamma}_0}\right)$, can be fitted to plots of the elastic and viscous stresses as a function of the strain (γ) and strain rate ($\dot{\gamma}$):

$$\sigma' = \gamma_0 \sum_{n=odd} e_n(\omega,\gamma_0)Tn\left(\frac{\gamma}{\gamma_0}\right) \tag{6}$$

$$\sigma'' = \dot{\gamma}_0 \sum_{n=odd} v_n(\omega,\dot{\gamma}_0)Tn\left(\frac{\dot{\gamma}}{\dot{\gamma}_0}\right). \tag{7}$$

For odd values of n, the elastic Chebyshev coefficient is given by $e_n = G'_n(-1)^{(n-1)/2}$ and the viscous Chebyshev coefficient is given by $v_n = \frac{G''_n}{\omega}$. Six categories of material viscoelastic behaviour

have been classified: strain-softening ($e_3 < 0$), linear elastic ($e_3 = 0$) and strain-stiffening ($e_3 > 0$) while the viscous behaviour is described as shear-thinning ($v_3 < 0$), linear viscous ($v_3 = 0$) and shear thickening ($v_3 > 0$). The FT-rheology package within TRIOS enabled direct extraction of the Chebyshev polynomial coefficients (e_n, v_n), for the selected harmonic number n. To create elastic and viscous Lissajous-Bowditch curves, data was acquired in the transient mode for fixed angular frequencies of $\omega = 0.1, 1$ and 10 rad/s and the amplitude of strain $\gamma_0 = 0.1\%, 1\%, 10\%, 100\%$ and 1000% for a sample of $\phi = 30\%$. These Pipkin maps provide a useful way to organise and classify the behaviour of viscoelastic and thixotropic materials. Prior to measurements on colloid-nematic dispersions, a 0.48%wt solution of xanthan gum in water was studied to verify the methodology reproducing the behaviour observed by Carmona *et al.* [13] and Ewoldt *et al.* [14].

III. RESULTS AND DISCUSSION

A. Optical microscopy

A confocal microscopy image of a dense ($\phi \sim 50\%$) dispersion in dodecane shows that particles do not aggregate in an isotropic solvent, as shown in Fig.2a. In Fig.2b, a single particle imaged using polarized optical microsopy reveals quadruplar distortion of the director field, indicating weak homeotropic anchoring of the director at the surface of the PMMA-PHSA particles [42]. A dispersion of $\phi = 33\%$ in 5CB, imaged through confocal microscopy reveals colloid aggregation and nematic (dark) domains of irregular shape and size $a \sim 10\mu$m, as shown in Fig.2c. A composite of $\phi = 30\%$, flattened between two untreated glass cover-slips with a gap $\sim 5\mu$m, imaged between crossed polarisers, is shown in Fig.2d. The nematic liquid crystal medium is birefringent appearing in various shades of grey, brightest (white) when the director is at 45°, and darkest (black) at 0°, to the polarisers. Isotropic particles appear as black circles and disclinations (having an isotropic core) appear as black lines connecting neighbouring particles. This provides the first direct experimental evidence of the network of disclinations that bind colloids, previously predicted through computer simulation, Fig.1b [1], formed when a concentrated colloid is mixed within the nematic phase [43].

Typical oscillatory strain sweep measurements, shown in Fig.3a, indicate that a $\phi = 28\%$ composite is highly elastic with $G' > G''$ in the linear viscoelastic region (LVR). The magnitude of the moduli are both $\sim 10^3$ Pa, remarkably, five orders higher than that for the pure liquid crys-

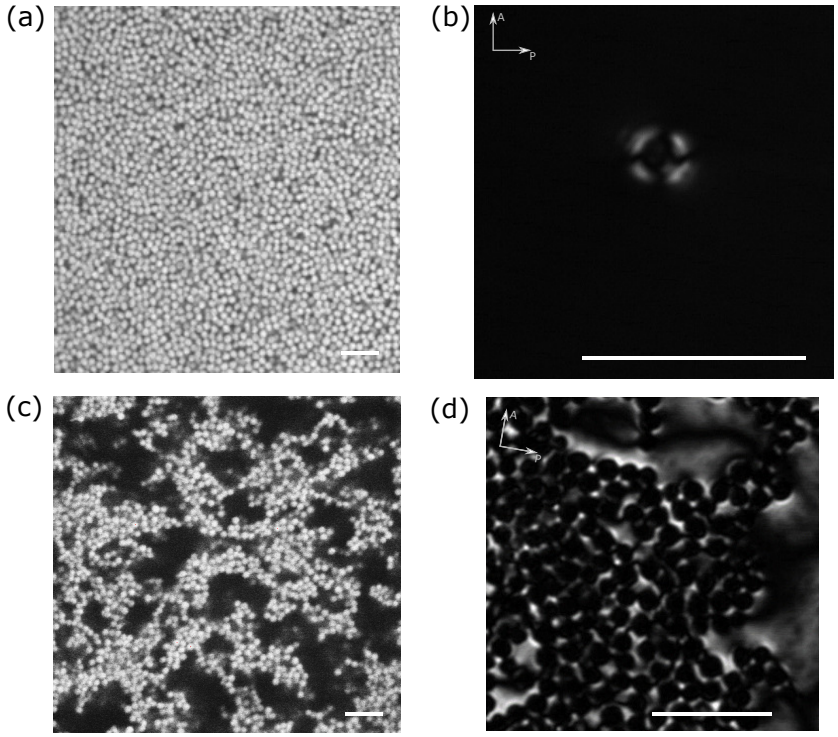

FIG. 2. a) A confocal microscopy image of the monodisperse PMMA-PHSA in dodecane. b) A polarized optical microscopy (POM) photograph of a single colloid dispersed in 5CB with the far-field director aligned with the analyser indicating quadrupolar distortion of the director at the particle surface. c) A confocal microscopy image of a $\phi = 33\%$ dispersion in 5CB. d) A POM image of a dispersion of $\phi = 30\%$ particles dispersed in 5CB, compressed to a sample thickness of $\sim 5\mu$m. Black lines connecting black circles provide direct evidence of disclinations linking neighbouring particles (both are isotropic within the birefringent background). All scale bars equal 6μm in length. For POM images, orientation of the orthogonal polariser (P) and analyser (A) are shown.

tal, $G'' \sim 10^{-2}$Pa and a concentrated ($\phi = 39\%$) dispersion in the isotropic solvent dodecane $G'' \sim 10^{-2}$Pa, also shown in Fig.3a.

Both cone-plate and plate-plate geometries generate the same values of γ_d and γ_c, as shown in Fig.3a. The magnitude of the moduli appear different, $G' \sim 400$Pa for $2r = 60$mm cone-plate and G' ~ 2000Pa for $2r = 40$mm. Recalling that $G' = T/d_{net}^2$, we find that d_{net} is around twice as large for the cone-plate geometry as for the plate-plate geometry. The similarity of the disclination density indicates that the disclinations bind well to both the sand-blasted steel parallel plates and the colloid-coated cone-plate geometries. Subsequent measurements for frequency sweep and LAOS measurements were performed with sand-blasted plates since they are more convenient to

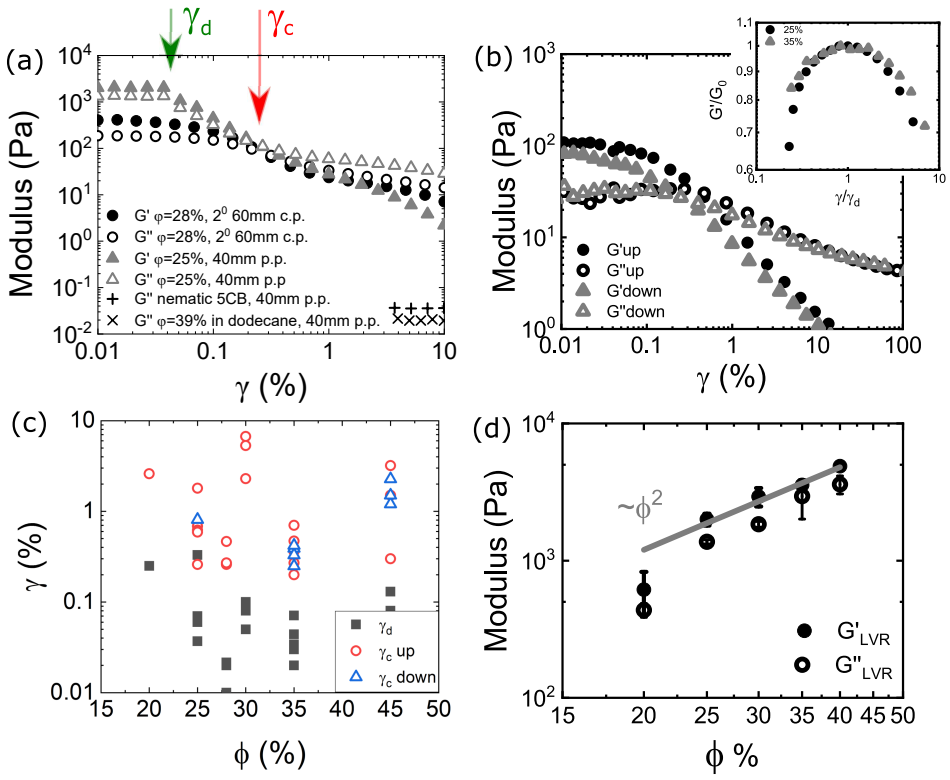

FIG. 3. a) The storage, G', and loss, G", moduli for oscillatory strain sweep measurements, at $\omega = 2\pi$rad/s, for $\phi = 25\%$ in nematic 5CB using 40mm diameter parallel plate geometry (grey triangles) and $\phi = 28\%$ in 5CB using a 2°, 60mm diameter cone-plate geometry (black circles), compared with the loss moduli for pure nematic 5CB and a $\phi = 39\%$ dispersion in the isotropic solvent dodecane. γ_d marks the end of the LVR for dispersions in nematic solvent, γ_c where $G' = G''$. b) 'Up' and 'down' sweeps for $\phi = 25\%$ on a cone-plate geometry indicate that the strain, $\gamma_c \sim 0.5\%$ for both sweeps although G' and G'' in LVR do not recover completely within the timescale of this experiment for the 'down' sweep. The inset shows that the normalised value of G'/G'_0 increases up to γ_d indicating strain hardening for both $\phi = 25\%$ and $\phi = 30\%$. c) γ_d is presented alongside γ_c for up and down sweeps for various samples across the range of ϕ and d) G'_{LVR} and G''_{LVR} measured for $\phi > 20\%$.

prepare and clean.

The LVR extends until a critical strain $\gamma_d \sim 0.1\%$ which is likely to be associated with the longer lengths of disclination within the composite, having a lengthscale $r_c/\gamma_d \sim 5\mu$m. Shorter 'figure of eight' disclinations of length d_0, are likely to yield at slightly larger strain amplitudes $\gamma_0 \sim r_c/d_0 \sim 0.4\%$. Within the LVR, there is evidence of strain-hardening since the storage modulus, normalised by its maximum value, G'/G'_0 increases before reaching the maximum at γ_d, as shown

in the inset of Fig.3b for $\phi = 25\%$ and $\phi = 30\%$. This suggests a resistance to deformation within the disclination bound structure. Since $G'_{LVR} \sim nT/A$ we deduce that the number of disclinations n spanning the composite decreases as the strain is increased beyond the LVR.

The direction of the amplitude sweep, as shown in Fig. 3b collected for ϕ = 25% composites on a cone-plate geometry for 'up' and 'down' sweeps, does not appear to affect the value of γ_c which has a wide range of values between $0.2\% < \gamma_c < 5\%$ and does not appear dependent on the volume fraction, as indicated in Fig. 3c. Visual observations under confocal microscopy, as shown in Fig. 2c, reveal that the microstructure is highly heterogeneous. Measurements of γ_c are highly scattered since the structure yields first in the weakest regions of the network then flows as clusters until the clusters break-up at high shear rates. The magnitude of the moduli takes around 1 minute to recover [1] which is beyond the timescale of this experiment ($\sim$ 10s per measurement) and therefore the measured $G'_{LVR}(\text{up}) > G'_{LVR}(\text{down})$.

As observed by Wood *et al.* [1] there is a rapid increase in the value of G' for $\phi \geq 18\%$, consistent with the functional form of $G'_{(LVR)}(\phi) \sim \phi^n$, with $n \sim 2$, see Fig.3d. Here, G'_{LVR} and G''_{LVR} values were calculated by averaging the value of the modulus for $\gamma_0 < \gamma_d$. Our measurements reveal that the loss modulus shows similar dependence, $G'' \sim \phi^2$, indicating that G'' and G' are intimately linked. If the number density of disclinations was determined solely by the particle diameter, we would expect $G' \sim T/d_{net}^2 \sim 100\text{pN}/1\mu\text{m}^2 \sim 100\text{Pa}$ but our experimental data shows $G' \rightarrow 4000\text{Pa}$ which suggests the disclination density $d_{net} \sim$ is close to one sixth of the particle diameter. It is known that complex knots and braids can be formed by disclinations weaving through a colloid in a nematic solvent in three dimensions [44]. Furthermore, a single Saturn-ring disclination could participate in multiple disclination pathways between the substrates in thus increasing the effective value for n. How these complex disclination structures contribute to the measured storage modulus is not known.

B. Frequency dependence

Within the plateau of the LVR, where the applied amplitude of strain $\gamma_0 < 0.1\%$, the oscillatory frequency sweep measurements indicate that $G' > G''$ with $\tan\delta = G''/G' = 0.86$ across all measurable frequencies down to 0.0004rad/s, as shown in Fig.4a. Samples stored in the laboratory for over a decade have remained stable, without phase separation, suggesting that $G' > G''$ for $\omega \rightarrow 10^{-8}$rad/s. From the rheology measurements it appears $G' > G''$ for over 7 orders of magni-

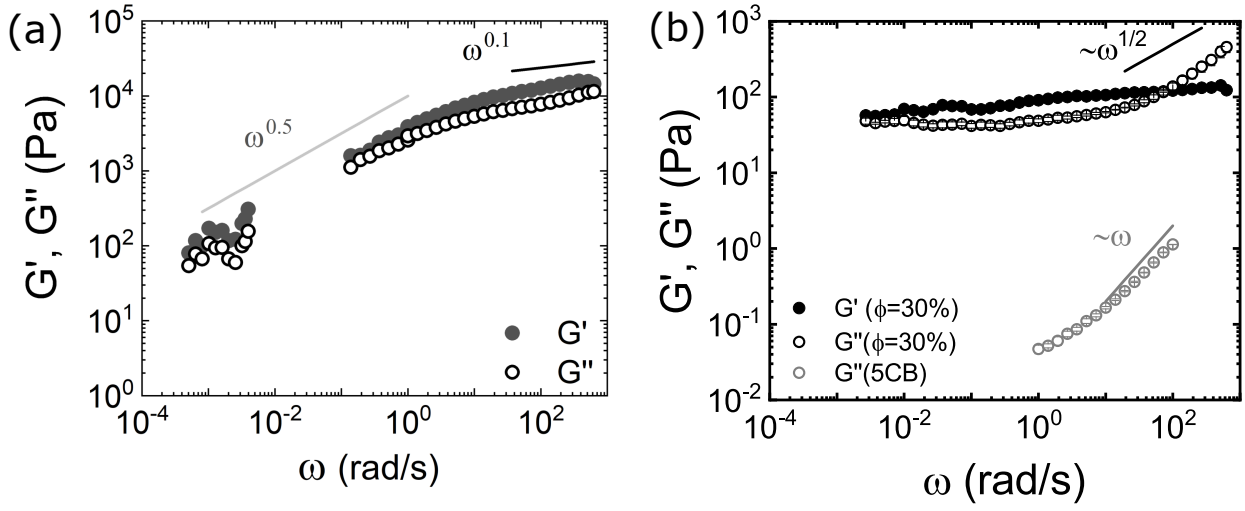

FIG. 4. Oscillatory frequency sweep measurement of a) $\phi = 30\%$ dispersion within the LVR at a strain of $\gamma = 0.1\%$. The frequency dependence is non-linear with G' and $G'' \sim \omega^{1/2}$ dependence at low frequencies and $\sim \omega^{0.1}$ at high frequencies but always $G' > G''$. b) A $\phi = 30\%$ dispersion in 5CB at a strain of $\gamma = 0.6\%$ shows $G' \sim \omega^{0.1}$ below a critical frequency ω_c, above which $G'' \sim \omega^{1/2}$ while for 5CB $G'' \to \omega$ (shown in grey).

tude in the angular frequency. Within the LVR, the amplitude of the applied strain is insufficient to break disclinations and $G' \sim G'' \sim \omega^{1/2}$ is observed at very low frequencies ($\omega < 1$ rad/s) satisfying the Kramers-Kronig relations [45]. The associated timescale of ~ 6.28s is commensurate with the time taken for a disclination to relax to its equilibrium position [25]. The gradient flattens at higher frequencies ($\sim \omega^{0.1}$) where the time for relaxation is insufficient. There is a gap in measured frequencies, as seen in Fig.4a, because each data point took over a day to collect at the lowest frequencies and it was impractical to measure the entire range.

To explore the yielding behaviour of this composite, we performed frequency sweep measurements just beyond the LVR where $\gamma_d < \gamma_0 < \gamma_c$, and discovered that G' and G'', are almost independent of the frequency $G \sim \omega^{0.1}$ until a critical frequency ω_c ($\omega_c \sim 10$ rad/s for $\gamma_0 = 0.6\%$) beyond which $G'' \sim \omega^{1/2}$, as shown in Fig.4b. Violation of the Kramers-Kronig relations has been observed in other driven and glassy systems [45]. This is unlike the frequency dependence of the pure liquid crystal (shown in grey), for which $G'' \sim \omega$ [21].

To compare multiple samples, it is more convenient to present the frequency response through $\tan\delta(\omega) = G''(\omega)/G'(\omega)$. Unexpectedly, the frequency response is independent of the colloid

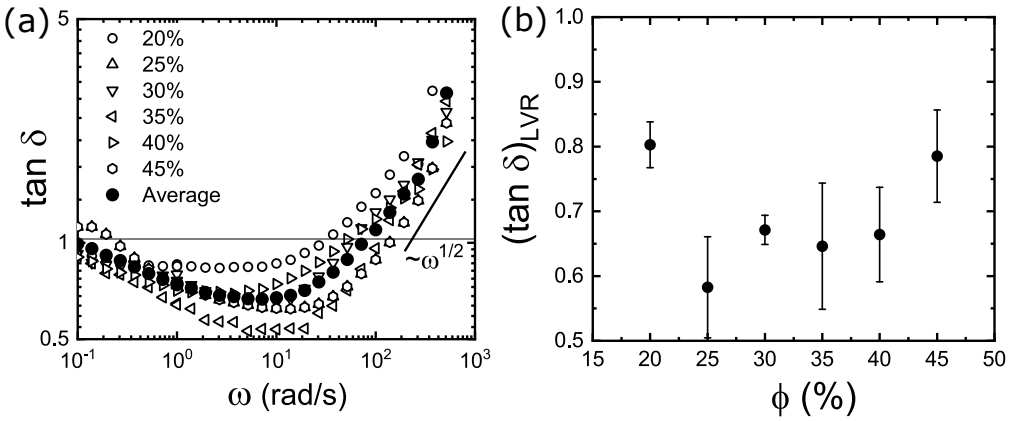

FIG. 5. a) An oscillatory frequency sweep of $\tan\delta = G''/G'$ at a strain of $\gamma = 0.6\%$ for the range in volume fraction of $20\% < \phi < 45\%$. b) The $\tan\delta$ value measured in the LVR across the range of volume fractions.

volume fraction, as shown in Fig.5a, showing no shift in the frequency at which $\tan\delta$ reaches a minimum (equivalent to $\frac{\mathrm{d}tan\delta}{\mathrm{d}\omega} = 0$) on increasing the filler concentration. This is very different to 'active' and 'passive' colloid-polymer systems [12] for which the frequency behaviour depends on volume fraction. In Fig.5b, we have plotted the LVR value of $\tan\delta_{LVR} = G''_{LVR}/G'_{LVR}$ as a function of volume fraction, ϕ. For all concentrations $0.6 < \tan\delta_{LVR} < 0.8$ and the standard deviation between repeat measurements is relatively large $\sim \pm 0.07$. However, aside from the lowest volume fraction measurement at $\phi = 20\%$, the data suggests that $\tan\delta_{LVR}$ may increase gradually with the volume fraction from a minimum at $\phi = 25\%$.

To explore the strain-dependent yielding behavior further, we repeated oscillatory frequency sweeps at $\omega = 2\pi$ rad/s at strain amplitudes beyond the LVR using a sample of $\phi = 30\%$. It was evident that the critical frequency ω_c at which G'' transitioned to $\sim \omega^{1/2}$ dependence reduced to lower frequencies when the strain amplitude was increased. Meanwhile G' remained almost independent of the frequency (similar to the result in Fig.4b) and therefore $\tan\delta \rightarrow \omega^{1/2}$ for $\omega > \omega_c$, as shown in Fig.6a. The critical frequency ω_c, at which $\tan\delta$ is at a minimum, i.e. where $\frac{\mathrm{d}tan\delta}{\mathrm{d}\omega} = 0$, is plotted in Fig.6b to reveal that $\omega_c \sim 1/\gamma_0$.

C. Large-amplitude oscillatory shear

To improve our understanding of how the structure yields beyond the LVR, LAOS data was acquired and the results are presented in Fig.7. In plots Fig.7b-e, the imposed strain and measured stress are plotted as a function of time during oscillation at $\omega = 2\pi$rad/s. For $\gamma_0 \sim \gamma_d$ ($\gamma_0 = 0.1\%$)

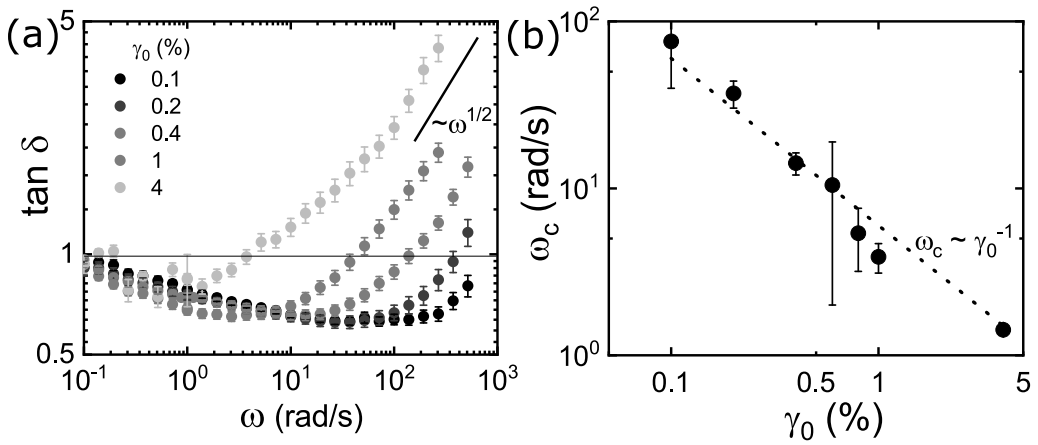

FIG. 6. a) tanδ as a function of angular frequency for $0.1\% < \gamma_0 < 4\%$ revealing that the frequency at which $\frac{\mathrm{d}tan\delta}{\mathrm{d}\omega} = 0$ is dependent on the strain amplitude γ_0. b) The critical frequency, ω_c beyond which $G'' \sim \omega^{1/2}$ is dependent on the strain amplitude following $\omega_c \sim 1/\gamma_0$

the measured stress, σ, is sinusoidal and close to being in phase with the strain indicating elastic behaviour. For $\gamma_d < \gamma_0 < \gamma_c$ (as represented by $\gamma_0 = 1\%$) the stress, σ is close to sinusoidal on increasing the strain but returns to zero, from the maximum strain amplitude γ_0, with a gradient that is steep and linear indicating the emergence of viscous behaviour. At $\gamma_0 = 10\%$ (close to γ_c) the phase difference between the stress and strain signal becomes large on the return journey from maximum strain γ_0 indicating viscous behaviour after yielding. At $\gamma_0 = 100\%$ ($> \gamma_c$) the phase difference between stress and strain is large at all times during the oscillation indicating that the flow behaviour is almost entirely viscous and has insufficient time to recover elasticity.

In Fig.7f it is evident that the higher order harmonics appear soon after $\gamma_0 = \gamma_d$ with the 3rd order elastic Chebyshev coefficient e_3 increasing, indicating strain-stiffening, until it reaches a maximum around γ_c beyond which it decreases to negative values consistent with strain-softening. The 3rd order viscous Chebyshev coefficient becomes negative beyond $\gamma_0 = \gamma_d$ indicating shear-thinning behaviour and reaches a minimum value at γ_c after which it returns towards zero, as shown in Fig.7g.

Elastic and viscous Lissajous-Bowditch curves, as presented in Fig.8, provide another way to present LAOS results and compare the 'rheological fingerprint' with systems studied previously. Within the LVR, a viscoelastic material is expected to have an elliptical shape as observed for $\gamma_0 = 0.1\%$ at all frequencies in both the elastic (Fig.8a) and viscous (Fig.8b) curves. Ewoldt *et al.* decomposed the elastic modulus into the minimum strain modulus G'_M, the tangent modulus

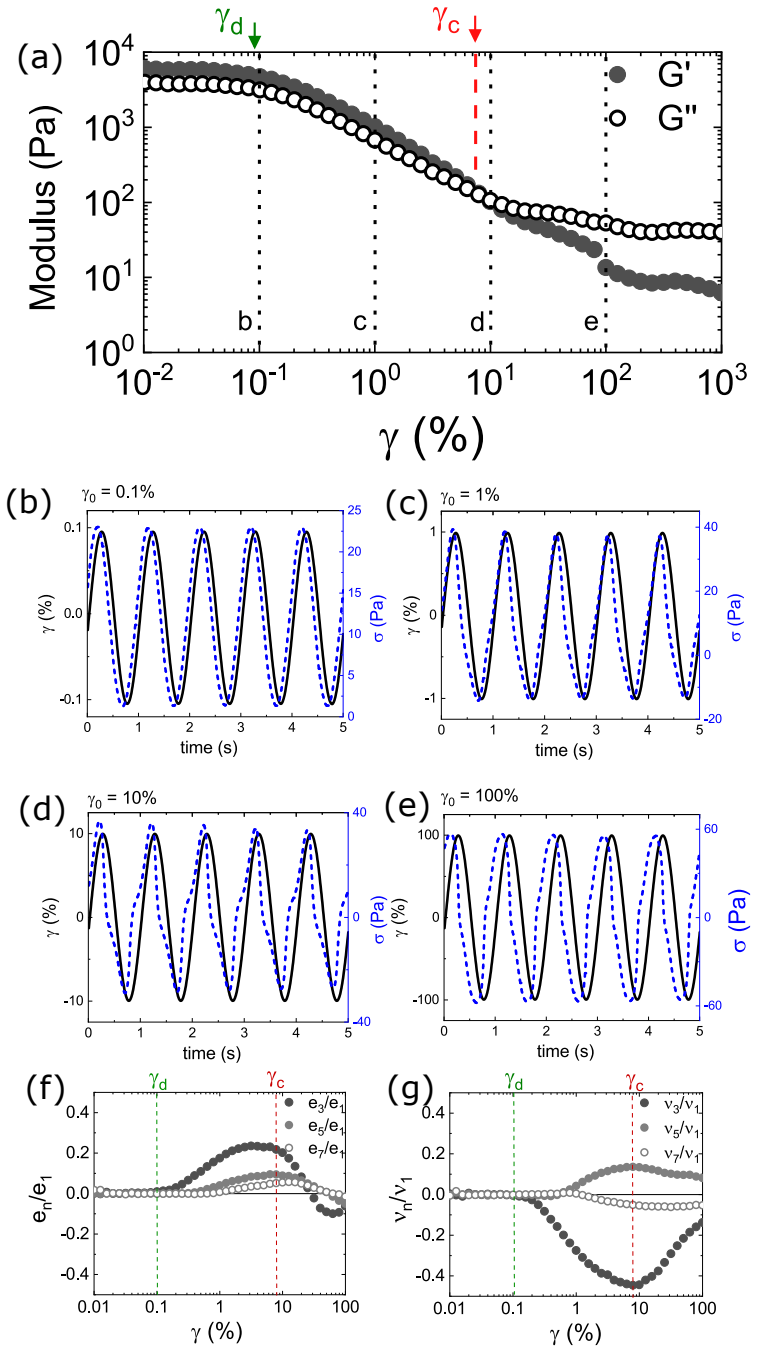

FIG. 7. a) The large amplitude oscillatory sweep for $\phi = 30\%$ showing the measured 1st order G' and G'' as a function of applied strain, critical strains γ_d (green) and γ_c (red) and fixed strain amplitudes (dotted blue lines) at which for b)-e), the imposed strain (black) and measured stress (blue) are plotted as a function of time at $\omega = 2\pi$rad/s. The maximum amplitudes γ_0 are 0.1% ($\sim \gamma_d$), 1% ($\gamma_d < \gamma_0 < \gamma_c$), 10% ($\sim \gamma_c$) and 100% ($> \gamma_c$) respectively. In f) the elastic e_n and in g) the viscous ν_n Chebyshev coefficients of the third, fifth and seventh order are plotted as a function of strain.

measured at $\gamma = 0$, and the large strain modulus, G'_L, the secant modulus measured at maximum strain that includes the signal from all odd Chebyshev harmonics [46]. Analogously, η'_L and η'_M indicate the instantaneous viscosity at the smallest and largest strain-rates, respectively.

A strain-hardening ratio, $S = \frac{G'_L - G'_M}{G'_L}$ and a shear thickening ratio $T = \frac{\eta'_L - \eta'_M}{\eta'_L}$ were defined by Ewoldt *et al.* [46]. Within the LVR, $G'_M = G'_L$ so that $S = 0$ and $\eta'_M = \eta'_L$ so that $T = 0$. At the maximum applied strain of $\gamma_0 = 1000\%$ $G'_L > G'_M$, such that $S > 0$, confirming intracycle strain-stiffening and $\eta'_L < \eta'_M$ such that $T < 0$ confirming intracycle shear thinning. The elastic and viscous Lissajous-Bowditch curves presented in Fig.8 are similar to a drilling fluid, reported by Ewoldt *et al.* in which a predominately elastic regime was observed at sufficiently small strain amplitude and an increasingly plastic regime at high strain magnitudes. Similarly, we deduce that a concentrated dispersion in a nematic solvent can be classed as an elastoplastic fluid. Small deformations allow the composite to maintain elasticity, larger deformations over long timescales (low frequencies) allow elasticity to be recovered, while large deformations and high shear rates (high frequencies) disrupt the structure irreversibly causing plastic deformation. More unusually, our measurements indicate a loss of symmetry about the stress axis at an intermediate strain of $\gamma_0 = 1\%$, occuring between the critical strains of γ_d and γ_c and higher angular frequencies $\omega > 0.1$ rad/s which can be attributed to hysteresis in the recovery of the gel strength due to the time taken for 'disclinations' to heal.

In summary, the rheology experiments on the yielding behaviour of colloidal dispersions in a nematic phase have revealed important and unusual phenomena:

- Dispersing a colloid within a nematic liquid crystal enhances the storage and loss moduli by over five orders of magnitude. This is remarkable in the context of other soft materials, for example an active filler in a polymer network increases the modulus by less than two orders of magnitude [12].

- For strain amplitudes within the LVR, $G' > G''$ for all measurable angular frequencies which is unusual since soft solids, in general, have experimentally accessible relaxation modes.

- For strain amplitudes beyond the LVR, the critical frequency ω_c for the onset of viscous behaviour is not affected by an increase in the colloid volume fraction ϕ. This is unusual since ω_c shifts for the majority of other soft composites, including dispersions in polymers [8] and emulsion systems [12] when the colloid concentration is increased.

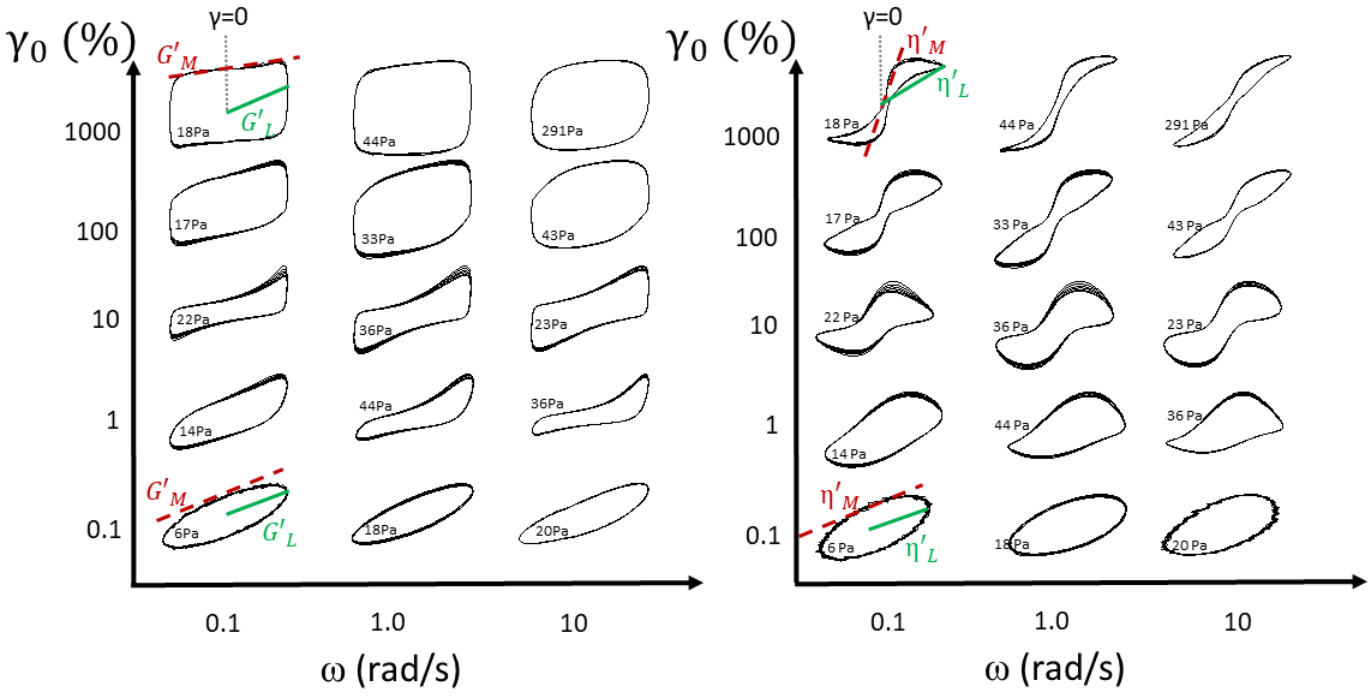

FIG. 8. a) Elastic Lissajous-Bowditch curves created from stress (y-axis) versus strain (x-axis) plots and b) viscous Lissajous-Bowditch curves created from stress (y-axis) versus strain-rate (x-axis) plots for fixed angular frequencies of $\omega = 0.1, 1$ and 10 rad/s and strain amplitudes $\gamma_0 = 0.1\%, 1\%, 10\%, 100\%$ and 1000% for $\phi = 30\%$.

- The end of the LVR occurs at unusually low strain amplitudes, $\gamma_d \sim 0.1\%$, much lower than the typical yield strain for a colloidal gel $\gamma_y \sim 10\%$ [11]. We attribute this yielding to reorientation of nematogens in the core of the disclination, of radius r_c with $\gamma_d \sim r_c/d$ where d is the distance between neighbouring colloid centres bound by entangled disclinations, limited by $d \to d_0$.

- For sufficient strain beyond the LVR and at frequencies above a critical frequency $\omega > \omega_c$, $G' \sim \omega^0$ and $G'' \to \omega^{1/2}$. This is novel behaviour for a nematic liquid crystal, very different from the $G'' \to \omega$ dependence observed for a pure nematic phase.

- A colloid dispersion in a nematic solvent can be classed as an elastoplastic that exhibits both strain-hardening and shear-thinning behaviour beyond the LVR.

D. Theoretical description of the yielding behaviour of defect-dominated gels in a nematic phase

To understand the experimental results we now consider the underpinning physics. As discussed in the introduction, the presence of a colloid with weak homeotropic anchoring gives rise to a Saturn-ring defect line, of topological charge $s = -\frac{1}{2}$ that, at sufficient colloid concentration, entangles with neighbouring Saturn ring disclinations, each providing a line tension T $\sim$ 100pN, to create numerous paths of continuous disclinations that extend throughout the sample, as illustrated in Fig.9a, to generate elasticity on a macroscopic scale.

The colloidal network is filled with pure nematic solvent, self-organizing to have an average domain size a, as illustrated in Fig.9b and observed experimentally in Fig.2c. Since each colloid surface and each disclination provide homeotropic anchoring, we expect each nematic domain to have radial alignment, although distorted due to the irregular shape of each domain. If the domain were circular, it would have a single central defect with topological charge, $S = 1$, as described by Terentjev *et al.*[27]. As the size of the domain reduces, it reaches a limiting size $a \sim K/W$ beyond which it is energetically unfavourable for the domain to reduce in size any further. This limit will drive structural rearrangements elsewhere in the system before a reduces further (e.g. at high colloid concentrations). We presume $W = 1.5X10^{-7}$ J/m^2, consistent with earlier estimations [27]. Using $K = 5.5$pN, we expect the magnitude of $a \sim 10\mu$m which is consistent with our experimental observations Fig.2c.

Existing equations describing the flow of liquid crystals have been derived for small amplitude oscillatory shear and we build upon this work. The storage modulus describes the elasticity of the material and, we presume, it is the sum of two contributions $G' = G'_f + G'_d$ for colloids dispersed in a nematic solvent. G'_f was described by Rey [21] and is the storage modulus arising from a nematic liquid crystal flowing between parallel plates. At frequencies greater than the resonance frequency ω_r it is given by

$$G'_f = \left(2\omega\eta_{bend} K \left(\frac{\alpha_2}{\gamma_r} \right)^2 \right)^{1/2} \tag{8}$$

where $\eta_{bend} = \gamma_r - \frac{\alpha_2^2}{\eta_2}$ and $\alpha_2 = -0.085$ Pa.s for 5CB [48]. We calculate $G'_f \sim 10^{-5}$Pa which is negligible compared with the storage modulus measured through experiment, therefore we assume $G' = G'_d$.

The storage modulus of a liquid crystal, caused by the presence of disclinations, at an average

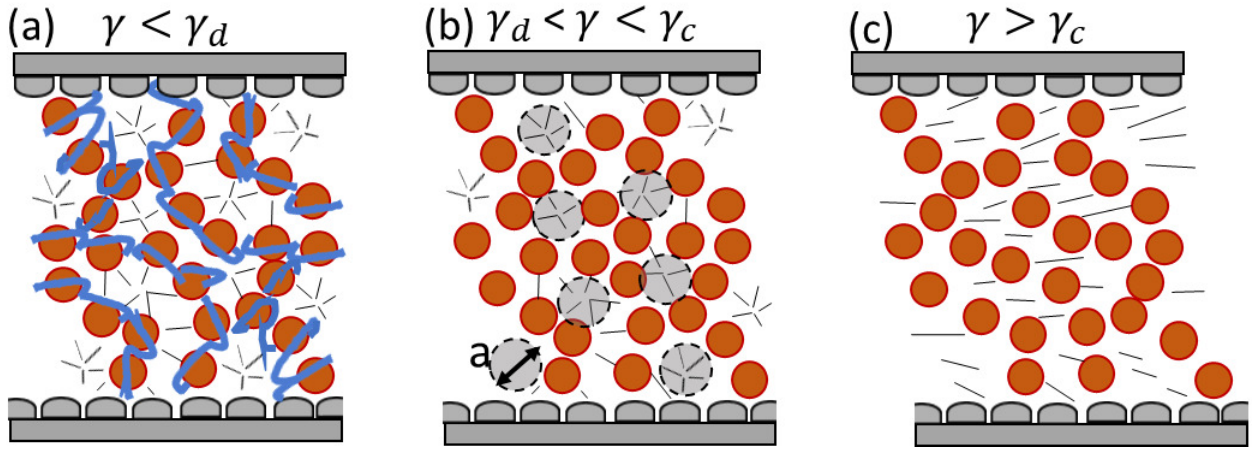

FIG. 9. Illustrations of a) disclinations (blue), encircling colloids (red) and connecting to create continuous disclinations extending across the sample, dominating the rheology for $\gamma < \gamma_d$; b) confined nematic regions (grey), with internal alignment (black lines) determined by the anchoring of nematogens normal to the colloid surfaces, dominate the rheology for $\gamma_d < \gamma < \gamma_c$ and c) at high shear $\gamma > \gamma_c$ nematogens will align with the direction of flow for the liquid crystal 5CB [47]

separation of d_{net}, was described by Weitz *et al.* [31] and Colby [3] as

$$G'_d = \frac{T}{d_{net}^2} \tag{9}$$

In the colloid-rich regions, we presume disclinations are separated by $d_0 = 1.1D$ where D is the diameter of the particles entanged by 'figure of eight' type disclinations. We assert that disclinations yield at a critical strain of $\gamma_d = \frac{r_c}{d_0}$ where r_c is the radius of the disclination core. Above this strain, disclinations yield such that the number density of disclinations decreases and the separation between disclinations increases as $d_{net} = \frac{d_0}{p(\phi)}\left(\frac{\gamma_d+\gamma}{\gamma_d}\right)$ following the empirical expression used by Colby *et al.* to describe the yielding behaviour of defect-mediated rheology for smectic liquid crystals [49]. This expression ensures $d_{net} \to d_0$ for very small strain amplitudes. A factor $p(\phi)$ has been introduced to match the model with experimental observations, likely to account for multiple entanglements within a three-dimensional network that increase with the volume fraction of colloids. We adopt the form $p(\phi) = p_{max}\left(\frac{(\phi-\phi_c)}{(\phi_{limit}-\phi_c)}\right)$. The resulting expression for G' is consistent with our observation that $G'_{LVR} \sim \phi^2$ and the correct magnitude of of $G'_{LVR}(\phi)$ is obtained when $p_{max} = 12$, $\phi_{limit} = 48\%$ and $\phi_c = 15\%$.

We presume the viscous behaviour of the composite is determined by two contributions $G'' =$

$G''_f + G''_a$. We assume the term, $G''_f = \eta_2 \omega$ describes the nematic flow behaviour at high shear where η_2 is the Miesovicz viscosity associated with the director aligning with the shear direction. G''_a describes the loss modulus enhanced within confined regions of nematic of size a.

The Ericksen number describes the competition between flow-induced and boundary-induced orientation within a nematic monodomain $E_r = \frac{L^2 \gamma_r \dot{\gamma}}{K}$ where γ_r is the rotational viscosity, $\dot{\gamma}$ is the shear rate and L is the relevant length scale. Reorientation of the director can occur when $E_r > 1$. For polydomains in liquid crystal polymers it has been argued that disclinations can act as an internal wall, similar to the colloid surfaces and together these structures provide boundaries with fixed homeotropic orientation [50]. Larson described the enhanced viscosity close to boundaries as $\eta_a \sim \gamma_r E r^{-1/2}$ [2]. Although there will be large nematic domains (without colloids) within the composite, as illustrated in Fig.9b, more confined nematic regions will contribute more significantly to G'' at low strain. In our model we assume $a = K/p(\phi)W$ to account for the enhanced confinement of the nematic liquid crystal due to the disclination density in the colloid-rich regions. This ensures $G''_{LVR} \sim \phi^2$, as observed through experiment and maintains the ratio between G'_{LVR} and G''_{LVR}, observed through experiment.

In oscillatory flow, the maximum shear rate $\dot{\gamma} = \gamma_0 \omega$ so that we can define the maximum Ericksen number during oscillatory flow as

$$E_r = \frac{a^2 \gamma_r \gamma_0 \omega}{2\pi K} \tag{10}$$

where a is the average size of nematic monodomains within the composite and is the appropriate lengthscale for confined regions of nematic fluid within the composite. The loss modulus can be described as $G''_a = \eta_a \omega$.

This expands to,

$$G''_a = \left(\frac{2\pi K \gamma_r \omega}{a^2 \gamma_0} \right)^{1/2} \tag{11}$$

This reveals that $G'' \sim \omega^{1/2}$ as observed experimentally at high frequencies. However, we have observed a critical frequency ω_c that must be overcome to allow flow to occur and therefore we replace $\omega \to \omega_c + \omega$ so that

$$G''_a = \left(\frac{2\pi K \gamma_r (\omega_c + \omega)}{a^2 \gamma_0} \right)^{1/2} \tag{12}$$

where $\omega_c = \frac{2\pi K}{a^2 \gamma_r \gamma_0}$ is the critical frequency at which flow occurs, as defined by the Ericksen number. This results in two components within the expression for G''_a which we simplify to $G''_a = G''_d + G''_c$. $G''_d = \frac{2\pi K}{a^2 \gamma_0}$ describes the plateau loss modulus at low frequencies $\omega < \omega_c$ while $G''_c = (G''_d \gamma_r \omega)^{1/2}$

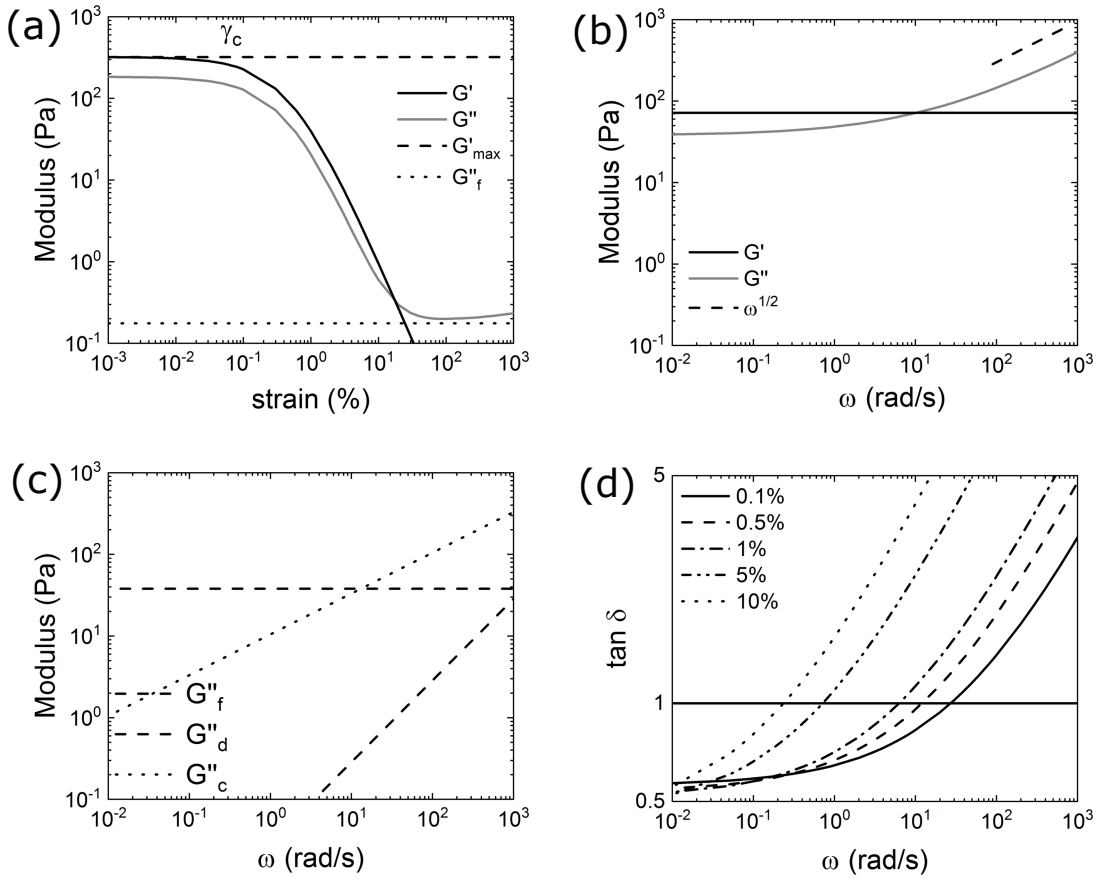

FIG. 10. a) Theoretical prediction of $G'(\gamma)$ and $G'(\gamma)$ for $\omega = 2\pi$ rad/s and b) $G'(\omega)$ and $G'(\omega)$ for $\gamma = 0.6\%$. c) Components G''_f, G''_d and G''_c contributing to the total loss modulus G'' shown in b). d) Plot of the theoretical $\tan\delta(\omega)$ for 0.1% to 10%. The parameters, $K = 5.5$pN, $W = 1.5 \times 10^{-7}$ J/m^2, $D = 2\mu$m and $\gamma_r = 81$ mPa.s, $r_c = 5$nm and $a = K/p(\phi)W$, with $\phi = 0.3$, $p_{max} = 12$, $\phi_{limit} = 48\%$ and $\phi_c = 15\%$, were used in this model.

becomes dominant at high frequencies $\omega > \omega_c$. To prevent the G'' from becoming unphysically large at very low strain we modelled the strain amplitude as $\gamma_0 \to (\gamma_0 + \gamma_d)^2/\gamma_d$.

The parameters, $K = 5.5$pN, $W = 1.5 \times 10^{-7}$ J/m^2, $D = 2\mu$m, $\gamma_r = 81$ mPa.s, $r_c = 5$nm and $a = K/p(\phi)W$ with $p_{max} = 12$, $\phi_{limit} = 48\%$ and $\phi_c = 15\%$, were used in the model. In Fig.10a the calculated G' and G'' as a function of the strain amplitude and Fig.10b in terms of the angular frequency, ω are presented. G' and G'' show strong similarities to the experimental results (Fig.3a) for increasing strain amplitude and frequency dependence (Fig.4b) with $G' > G''$ at low frequencies and $G'' \sim \omega^{1/2}$ above a critical frequency. The magnitude of the individual components of G''_d, G''_c and G''_f are compared in Fig.10c. It is clear that for confined regions $G''_d \gg G''_f$ so that

$G'' \sim \omega^{1/2}$ although there is an underlying $G''_f \sim \omega$ dependence that would dominate if a were sufficiently large [31].

Fig.10d the theoretical contribution of $\tan\delta = G''/G'$ is shown for a range of applied strain amplitudes ($0.1\% < \gamma_0 < 10\%$) as a function of the angular frequency and reveals similar behaviour to experimental measurements presented in Fig.6b. At low frequencies ($\omega < \omega_c$), $\tan\delta = G''/G'$ takes the equation form,

$$tan\delta(\omega < \omega_c) = \frac{2\pi K}{T}\frac{1}{\gamma_0}\frac{d_{net}^2}{a^2}. \tag{13}$$

This indicates that $\tan\delta(\omega < \omega_c)$ is dependent on the square of the ratio of the size of the disclination spacing to the nematic domain size d_{net}/a. If we substitute $a \sim K/p(\phi)W$ and $d_{net} = d_0/p(\phi)$, within the LVR the expression can be simplified further to $\tan\delta \sim \frac{2\pi}{\gamma_0}\frac{W^2 d_0^2}{TK}$. This reveals that the anchoring strength W of nematogens at the surface of the colloid, having homeotropic alignment, has a significant influence on the flow properties of the composite. This expression for $\tan\delta$ is independent of the volume fraction ϕ although there may more complexity since $\tan\delta$ increased slightly with volume fraction, as revealed in Fig.5b, potentially due to crowding.

Despite the progress made through matching the experimental measurements with a simple theoretical model there are opportunities to refine the model, perhaps best tackled through computer simulation.

- Following the work of Muševic [44] it may be possible for theoreticians to determine the average separation between disclinations d_{net} binding a dense suspension of colloids within a nematic solvent in three dimensions to improve our understanding of $p(\phi)$.

- Experiments indiciate that at high shear $G'' \to 10^2$ Pa, not $G'' \to \eta_2\omega \sim 10^{-1}$Pa as assumed in the simple theory presented here. Inter-particle interactions must persist within the nematic phase under flow to enhance the viscosity of the filled nematic at high shear and this is a complex problem to solve.

- 4-Cyano-4'pentylbiphenyl (5CB) is a flow-aligning nematic liquid crystal but others, e.g. 4-Cyano-4'heptylbiphenyl (7CB) tumble at high shear [47]. The effect of potential tumbling behaviour on the rheology of colloid-nematic composites is unknown.

- This model describes the yielding behaviour of the composite at intermediate strain amplitudes for which rheology measurements indicate that $G'(\omega) \sim \omega^0$ and $G'(\omega) \sim \omega^{1/2}$, as revealed in Fig.4b. It does not explain the $G'(\omega) \sim G''(\omega) \sim \omega^{1/2}$ behaviour observed

at very low strain amplitudes, well within the LVR, as shown in Fig.4b which requires an expression for G' that captures the dynamics of disclination relaxation.

Interestingly, through performing oscillatory rheology on colloidal dispersions in small-molecule nematic liquid crystalline materials we have observed two regimes that are analogous to defect-dominated flow behaviour observed in nematic liquid crystal polymer (LCP) systems for which various regimes have been reported [3, 51]. Regime 0 is associated with viscosity dependence $\eta \sim \dot{\gamma}^{-1}$ and is attributed to the solid like response at very low shear rates. Regime 1 is associated with viscosity behaviour $\eta \propto \dot{\gamma}^{-1/2}$ and is attributed to the movement of disclinations within the LCP [3]. Similar to our colloidal network interpenetrated by multiple nematic domains of size a, these LCPs have a poly-domain texture [5, 52, 53]. A complex viscosity, η^* can be determined from oscillatory measurements using $\eta^* = \frac{(G'^2+G''^2)^{1/2}}{\omega}$. For our confined nematic solvent, made of small-molecule nematogens, experimental measurements show that $G' \sim \omega^0$ for all frequencies. At very low shear rates, $G'' \sim \omega^0$ such that $\eta^* \sim \omega^{-1}$. Above the critical frequency, associated with higher shear rates, $G'' \sim \omega^{1/2}$ and thereafter $G'' > G'$ so that $\eta^* \to \omega^{-1/2}$. The similarity to our experimental results is intriguing because it suggests that the low shear behaviour of a LCP could be attributed to the behaviour of nematogens in confinement.

Furthermore, the $G'' \sim \omega^{1/2}$ behaviour explained through our experiments has been observed in a myriad of defect-dominated liquid crystalline systems aside from LCPs including a thermotropic smectic [49], a lamellar lyotropic liquid crystal [54], and dispersions of colloids in a thermotropic smectic [4], in a nematic [32] and in a cholesteric [55] for which the principles explained in this paper are applicable. However, it is important to bear in mind that this behaviour will only occur in systems that support a sufficiently high density of disclinations and therefore $G'' \sim \omega^{1/2}$ dependence has not been observed in pure cholesteric phases [31], liquid crystal polymers that retain good nematic alignment [5] or for dispersions in the nematic phase that do not give rise to weak quadrupolar anchoring at the colloid surface [56] since this is an essential condition for generating networks bound by entangled disclinations.

IV. CONCLUSION

In conclusion, we bring SAOS and LAOS experiments together with a simple theory to explore the dynamic behaviour of an extraordinarily stable soft-solid formed upon dispersing colloids, of volume fractions $18\% < \phi < 45\%$, in a nematic phase where nematogens are weakly oriented per-

pendicular to the colloid surface. LAOS reveals that the shear-thinning behaviour associated with the breakage of disclinations is accompanied by strain-hardening due to the resistance of nematic domains to deformation. Although the magnitude of the storage, G', and loss G'' moduli, $\sim \phi^2$, the volume fraction has no effect on the critical frequency ω_c associated with yielding, where $G'' = G'$. Instead, the critical frequency ω_c is sensitive to the disclination density d_{net}, the size of entrapped nematic domains a, the generalized Frank elastic constant K and, most importantly, the anchoring strength W through which nematogens are associated with the surface of the colloid. Reorientation of the director is only permitted if the $E_r > 1$ and, in a defect-mediated structure $E_r \sim \frac{\gamma_r a^2 \dot{\gamma}_0}{K}$ where γ_r is the rotational viscosity of the nematic phase and $\dot{\gamma}_0$ is the maximum shear rate, equivalent to $\gamma_0 \omega / 2\pi$. Beyond ω_c the viscous behavior $G'' \sim \omega^{1/2}$ due to the enhanced viscosity of a nematic liquid crystal in regions confined by the colloidal network, behaviour that has also been observed for other defect mediated liquid crystalline structures [3, 51, 52]. Experimental observation of this behaviour within a small-molecule nematic liquid crystalline phase has allowed us to develop a simple theory for both elastic and viscous contributions and extends our understanding of the flow behaviour of defect-mediated liquid crystalline materials. This fascinating class of glassy soft-solid [57] has received scant attention to date and our work could provide guidelines for developing new composites with superior physical stability.

ACKNOWLEDGMENTS

We thank Professors Davide Marenduzzo and Wilson C. K. Poon for insightful discussions over several years. This work was funded by a Royal Society Industry Fellowship, grant number IF140071, and a Sydney-Andrew Scholarship awarded by the Society of Chemical Industry (SCI).

REFERENCES

[1]T. A. Wood, J. S. Lintuvuori, A. B. Schofield, D. Marenduzzo, and W. C. K. Poon, "A self-quenched defect glass in a colloid-nematic liquid crystal composite," Science **334**, 79–83 (2011).

[2]R. G. Larson, *The structure and rheology of complex fluids* (Oxford University Press, 1999) p. 463.

[3]R. H. Colby, "Defect-mediated creep of structured materials," Europhysics Letters **54**, 269–274 (2001).

[4]R. Sahoo and S. Dhara, "Rheological studies on liquid-crystal colloids prepared by dispersing spherical microparticles with homeotropic surface anchoring," Liquid Crystals **44**, 1582 (2017).

[5]A. Romo-Uribe, "Shear-induced textures and viscoelasticity in the nematic and isotropic phase of semiflexible thermotropic polymers. A rheo-optical study," Polymers Advanced Technologies **32**, 651–662 (2021).

[6]J. Bergenholtz, W. C. K. Poon, and M. Fuchs, "Gelation in model colloid-polymer mixtures," Langmuir **19**, 4493–4503 (2003).

[7]P. Poulin, H. Stark, T. C. Lubensky, and D. A. Weitz, "Novel colloidal interactions in anisotropic fluids," Science **275**, 1770–1773 (1997).

[8]S. Weir, K. M. Bromley, A. Lips, and W. C. K. Poon, "Celebrating soft matter's 10th anniversary: Simplicity in complexity – towards a soft matter physics of caramel," Soft Matter **12**, 2757–2765 (2016).

[9]J. D. Ferry, *Viscoelastic Properties of Polymers* (Wiley, 3rd edn, 1980).

[10]S. S. Datta, D. D. Gerrard, T. S. Rhodes, T. G. Mason, and D. A. Weitz, "Rheology of attractive emulsions," Physical Review E **84**, 041404 (2011).

[11]K. N. Pham, G. Petekidis, D. Vlassopoulos, S. Egelhaaf, W. Poon, and P. N. Pusey, "Yielding behaviour of repulsion- and attraction-dominated colloidal glasses," Journal of Rheology **52**, 649–676 (2008).

[12]E. Dickinson and J. Chen, "Heat-set whey protein emulsion gels: Role of active and inactive filler particles," Journal of Dispersion Science and Technology **20**, 197–213 (1999).

[13]J. Carmona, P. Ramírez, N. Calero, and J. Muñoz, "Large amplitude oscillatory shear of xanthan gum solutions. Effect of sodium chloride (NaCl) concentration," Journal of Food Engineering **126**, 165–172 (2014).

[14]R. H. Ewoldt, P. Winter, J. Maxey, and G. H. McKinley, "Large amplitude oscillatory shear of pseudoplastic and elastoviscoplastic materials," Rheologica Acta **49**, 191–212 (2010).

[15]E. Y. X. Ong, M. Ramaswamy, R. Niu, N. Y. C. Lin, A. Shetty, R. N. Zia, G. H. McKinley, and I. Cohen, "Stress decomposition in LAOS of dense colloidal suspensions," Journal of Rheology **64**, 343 (2020).

[16]A. K. Gurnon and N. J. Wagner, "Large amplitude oscillatory shear (LAOS) measurements to obtain constitutive equation model parameters: Giesekus model of banding and nonbanding wormlike micelles," Journal of Rheology **56**, 333 (2012).

[17]P. G. de Gennes and J. Prost, *The Physics of Liquid Crystals*, 2nd ed., International Series of Monographs on Physics 83 (Clarendon Press, 1993).

[18]W. W. Beens and W. H. de Jeu, "Flow-measurements of the viscosity coefficients of two nematic liquid crystalline azoxybenzenes," Journal Physique **44**, 129–136 (1995).

[19]W. R. Burghardt, "Oscillatory shear flow of nematic liquid crystals," Journal of Rheology **35**, 49–62 (1991).

[20]P. T. Mather, D. S. Pearson, and R. G. Larson, "Flow patterns and disclination-density measurements in sheared nematic liquid crystals I: Flow-aligning 5CB," Liquid Crystals **20**, 527–538 (1996).

[21]L. R. de Andrade Lima and A. Rey, "Superposition principles for small amplitude oscillatory shearing of nematic mesophases," Rheologica Acta **45**, 591–600 (2006).

[22]P. T. Mather, D. S. Pearson, and W. R. Burghardt, "Structural response of nematic liquid crystals to weak transient shear flows," Journal of Rheology **39**, 627–648 (1995).

[23]D. J. Ternet, R. G. Larson, and L. G. Leal, "Transient director patterns upon flow start-up of nematic liquid crystals," Rheologica Acta **38**, 183 (2000).

[24]J. Nehring and A. Saupe, "On the elastic theory ofiaxial liquid crystals," The Journal of Chemical Physics **54**, 337–343 (1971).

[25]N. Osterman, J. Kotar, E. M. Terentjev, and P. Cicuta, "Relaxation kinetics of stretched disclination lines in a nematic liquid crystal," Physical Review E **81**, 061701 (2010).

[26]M. Škarabot, M. Ravnik, S. Žumer, U. Tkalec, I. Poberaj, D. Babič, N. Osterman, and I. Muševic, "Interactions of quadrupolar nematic colloids," Physical Review E **77**, 031705 (2008).

[27]E. M. Terentjev, "Disclination loops, standing alone and around solid particles, in nematic liquid crystals," Physical Review E **51**, 1330–1337 (1995).

[28]H. Y. J. Fukuda, "Nematic liquid crystal around a spherical particle: Investigation of the defect structure and its stability using adaptive mesh refinement," European Physical Journal E **38**, 87–98 (2004).

[29]Y. Gu and N. L. Abbott, "Observation of saturn-ring defects around solid microspheres in nematic liquid crystals," Physical Review Letters **85**, 4719–4722 (2000).

[30]T. Araki and H. Tanaka, "Colloidal aggregation in a nematic liquid crystal: Topological arrest of particles by a single-stroke disclination line," Physical Review Letters **97**, 127801 (2006).

[31]L. Ramos, M. Zapotocky, T. C. Lubensky, and D. A. Weitz, "Rheology of defect networks in cholesteric liquid crystals," Phys. Rev. E **66**, 031711 (2002).

[32]S. Kumar, S. Khatua, and P. Thareja, "Fumed alumina-in-nematic liquid crystal suspensions under shear and electric field," Rheologica Acta **58**, 203–216 (2019).

[33]S. Alama, L. Bronsard, and X. Lamy, "Analytical description of the saturn-ring defect in nematic colloids," Physical Review E **93**, 012705 (2016).

[34]L. Antl, J. W. Goodwin, R. D. Hill, R. H. Ottewill, S. M. Owens, S. Papworth, and J. A. Waters, "The preparation of poly(methyl methacrylate) latices in non-aqueous media," Colloids and Surfaces **17**, 67–78 (1986).

[35]G. Bosma, C. Pathmamanoharan, E. H. A. de Hoog, W. K. Kegel, A. van Blaaderen, and H. N. W. Lekkerkerker, "Preparation of monodisperse, fluorescent PMMA-latex colloids by dispersion polymerization," Journal of Colloid and Interface Science **245**, 292–300 (2002).

[36]N. Lebovka, A. Melnyk, Y. Mamunya, G. Klishevich, A. Goncharuk, and N. Pivovarova, "Low temperature phase transformations in 4-cyano-4'-pentylbiphenyl (5CB) filled by multiwalled carbon nanotubes," Physica E **52**, 65–69 (2013).

[37]E. Nowinowski-Kruszelnicki, J. Kedzierski, Z. Raszewski, L. Jaroszewicz, M. A. Kojdecki, W. Piecek, P. Perkowski, M. Olifierczuk, and E. Miszczyk, "Measurements of elastic constants of nematic liquid crystals with use of hybrid in-plane-switched cell," Opto-electronics Review **20**, 255–259 (2012).

[38]S. Zhou, K. Neupane, Y. A. Nastishin, A. R. Baldwin, S. V. Shiyanovskii, O. D. Lavrentovich, and S. Sprunt, "Elasticity, viscosity and orientational fluctuations of a lyotropic chromonic nematic liquid crystal disodium cromoglycate," Soft Matter **10**, 6571–6581 (2014).

[39]M. L. Dark, M. H. Moore, D. K. Shenoy, and R. Shashidhar, "Rotational viscosity and molecular structure of nematic liquid crystals," Liquid Crystals **33**, 67–73 (2006).

[40]H. Chen, C. Xu, G. Xiao, Z. Chen, M. Yi, and J. Zhang, "Surface anchoring behaviour of 5CB liquid crystal confined between iron surfaces: A molecular dynamics study," Applied Surfaces Science **508**, 145284 (2020).

[41]K. S. Cho, K. Hyun, K. H. Ahn, and S. J. Lee, "A geometrical interpretation of large amplitude oscillatory shear response," Journal of Rheology **49**, 747 (2005).

[42]J. C. Loudet, P. Barois, P. Aurov, P. Keller, H. Richard, and P. Poulin, "Colloidal structures from bulk demixing in liquid crystals," Langmuir **20**, 11336–11347 (2004).

[43]V. Anderson, E. M. Teretjev, S. P. Meeker, J. Crain, and W. C. K. Poon, "Cellular solid behaviour of liquid crystal colloids 1. Phase separation and morphology," The European Physical Journal E **4**, 11–20 (2001).

[44]I. Muševic, "Interactions, topology and photonic properties of liquid crystal colloids and dispersions," European Physical Journal Special Topics 2 **227**, 2455–2485 (2019).

[45]Y. H. Wen, J. L. Schaefer, and L. A. Archer, "Dynamics and rheology of soft colloidal glasses," ACS Macro Letters **4**, 119–123 (2015).

[46]R. H. Ewoldt, A. E. Hosoi, and G. H. McKinley, "New measures for characterizing nonlinear viscoelasticity in large amplitude oscillatory shear," Journal of Rheology **52**, 1427 (2008).

[47]D. J. Tenet, R. G. Larson, and L. G. Leal, "Flow-aligning and tumbling in small-molecule liquid crystals: pure components and mixtures," Rheologica Acta **38**, 183–197 (1999).

[48]M. Cui and J. R. Kelly, "Temperature dependence of visco-elastic properties of 5CB," Molecular Crystals and Liquid Crystals **331**, 49–57 (1999).

[49]R. H. Colby, C. H. Ober, J. R. Gillmor, R. W. Connelly, T. Duong, G. Galli, and M. Laus, "Smectic rheology," Rheologica Acta **36**, 498–504 (1997).

[50]D. Acierno and A. Collyer, *Rheology and Processing of Liquid Crystal Polymer* (Springer Science, 1996) p. 41.

[51]L. Walker and N. Wagner, "Rheology of region I flow in a lyotropic liquid-crystal polymer: The effects of defect texture," Journal of Rheology **38**, 1525 (1994).

[52]G. M. G. Astarita and L. Nicolais, *Rheology Principles* (Plenum Press, 1980) p. 136.

[53]E. Somma, R. Iervolino, and M. Rosselle Nobile, "The viscoelasticity of thermotropic liquid crystalline polymers: effects of the chemical composition," Rheologica Acta **45**, 486–496 (2006).

[54]R. G. Larson and D. W. Mead, "Linear viscoelasticty of nematic liquid crystalline polymers," Journal of Rheology **33**, 185 (1989).

[55]M. Zaptocky, L. Ramos, P. Poulin, T. C. Lubensky, and D. A. Weitz, "Particle-stabilized defect gel in cholesteric liquid crystals," Science **283**, 209 (1999).

[56]Z. Liu and W. Yu, "Linear and nonlinear rheology of oil in liquid crystal emulsions," Rheologica Acta **59**, 783–795 (2020).

[57]P. Sollich, F. Lequeux, P. Hébraud, and M. E. Cates, "Rheology of soft glassy materials," Physical Review Letters **78**, 2020–2023 (1997).